

Degradation Benefits Polymerization: Photo-Generated Self-Degradable Organo-Catalyst for Higher-Efficiency ATRP and Pure Polymers

Yan Luo,^a Lingpu Jia,^b Yanghong Xu,^a Enmin Hu,^a Meekyung Song,^c Xiaofeng Zhu,^a Youngsoo Kang,^c Yun Huang,^d Long Yang,^{a, c*}

^a State Key Laboratory of Environment-Friendly Energy Materials, School of Materials and Chemistry, Southwest University of Science and Technology, Mianyang 621010, Sichuan, China. Email: yanglong@swust.edu.cn

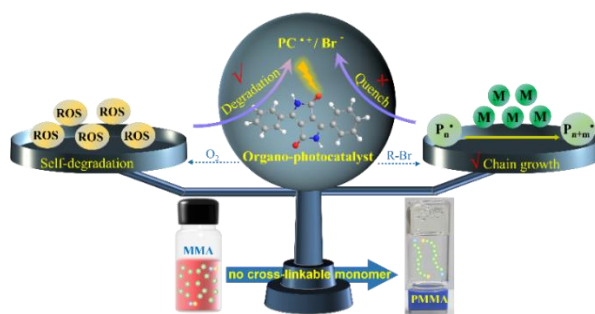
^b Key Laboratory of Medicinal and Edible Plants Resources Development of Sichuan Education Department, Institute for Advanced Study, Chengdu University, Chengdu 610106, China

^c Environmental and Climate Technology, Korea Institute of Energy Technology (KENTECH), 200 Hyeoksins-ro, Naju 58330, Republic of Korea.

^d State Key Laboratory of Polymer Materials Engineering of China (Sichuan University), Polymer Research Institute of Sichuan University, Chengdu 610065, China.

KEYWORDS: Organo-photocatalyst; Ultra-high molecular weight; Pure polymer; Degradation; ATRP.

ABSTRACT: In the realm of polymer-based 3D photo printing, challenges arise from the side effects, notably the persistent presence of photocatalyst residues and metal contamination. These impurities pose significant risks in various applications, including electronics, biological tissues, and medical implants. At the same time, spatial-/time-/light-controlled 3D photo printing has been hindered by low-efficiency polymerization concerning both initiation and monomer conversion. To address these critical issues, a pioneering concept, “degradation-inhibited quench,” is introduced and implemented within photopolymerization to solve the problems mentioned above. This innovative approach aims to produce pure polymers via higher-efficiency Atom Transfer Radical Polymerization (ATRP) with a unique class of diketopyrrolopyrrole (DPP) derivatives as organo-photocatalysts at an extremely low concentration (as low as 50ppm). Through this approach, pure polymers with ultra-high molecular weight (UHMW) have been successfully synthesized. For instance, poly(methyl methacrylate) (PMMA) achieved a monomer conversion of > 50%, a molecular weight of 2.1 million, and a dispersity of 1.38 after 12 h additional dark reaction. Notably, this novel photopolymerization method demonstrates applicability across a broad spectrum of monomers, with or without solvents, including acrylate, acrylic, styrene, and acrylonitrile. Mechanism insights revealed that the production of UHMW PMMA stemmed from the degradation of intermediate complex $DPP^{•+}/Br^-$, which originated from the photo initiation. This degradation inhibited the oxidative quenching of active propagating chain radicals, thereby significantly extending their lifespan. This groundbreaking concept embraces the potential for further development of highly effective organo-photocatalysts and reactive systems specifically tailored for 3D photopolymerization. Moreover, this novel spatial-/time-/light-controlled polymerization approach does not require any additional purification, offering energy and cost-saving manufacturing technology.



A novel degradation-inhibited-quench effect was applied in photopolymerization to produce pristine polymers with ultra-high molecular weight by manipulating the organo-photocatalyst intermediate's reaction.

Introduction

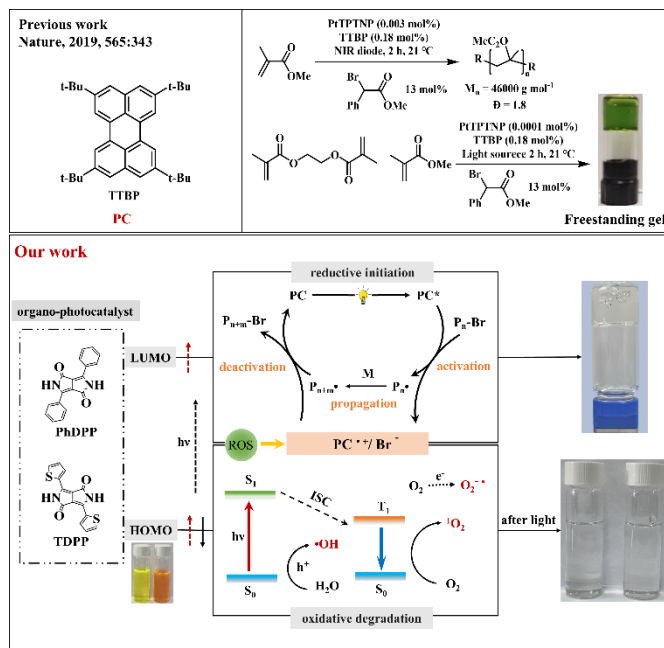
In the past decade, the field of 3D printing technology has experienced significant progress across a multitude of application domains.¹⁻³ Among numerous 3D printing methods, the photochemical approach stands out due to its capability to fabricate objects through monomers/oligomers photopolymerization reactions, offering notable advantages in terms of environmental sustainability and economic efficiency.⁴⁻⁶ Therefore, photo-induced polymerization emerges as a particularly promising technique for 3D-printing applications, as it allows for precise control over light exposure, spatial arrangement, and time at room temperature.⁷⁻⁸ However, the application of the 3D photo printing technique in critical sectors like tissue engineering and electrical components has been hindered. Challenges such as metal contamination, catalyst residue, toxicity, and color retention have been noted in association with many reported photo-initiator systems.⁹

The need to remove photocatalysts (PCs) and obtain pure polymer products during the 3D photo printing process is urgent and crucial, especially for applications relying on polymers that can only be made from photopolymerization.¹⁰⁻¹² Despite this urgency, this photopolymerization process also has been plagued by low reaction efficiency, partially in the initiation and monomer conversion stages. Noteworthy efforts have been made in this area. For instance, Miyake¹³ and his colleagues successfully prepared PMMA by utilizing 5,10-diphenyl-5,10-dihydrophenazines as a photocatalyst and ethyl α -bromophenylacetate (EBP) as an initiator, achieving notable dispersion and initiator efficiencies of 1.23 and 99.3%, respectively. Similarly, Congreve¹⁴ et al. synthesized gel-form PMMA using tetratertbutylperylene (TTBP). However, these polymers retained residual catalysts and suffered color retention issues, leading to additional discoloration. The elimination of catalysts used in photopolymerization has been inherently challenging, and current purification techniques predominantly rely on precipitation, which cannot be implemented for producing thermosets in 3D photopolymerization. While reducing the catalyst loading can mitigate contamination and residue, it substantially decelerates the kinetics of the polymerization reaction. Therefore, a pressing need for a technique that efficiently eliminates residual PCs while ensuring continued polymer chain growth. This method is crucial to attain pure polymers through highly efficient photopolymerization, obviating the necessity for excessive purification processes.

In this study, we propose the utilization of organo-photocatalyst self-degradation and simultaneous monomer initiation and chain growth to produce pure polymers by photo-redox, a concept defined as degradation-inhibited quench. Based on our in-depth understanding of photopolymerization¹⁵ and the structure-performance relationship of organo-photocatalysts,¹⁶⁻¹⁷ we have deliberately chosen N-unsubstituted diketopyrrolopyrrole (DPP) derivatives as catalysts for visible-light-induced polymerization systems, diverging from the commonly reported N-alkyl-substituted DPP. In the photopolymerization process, the key intermediate to control the balance of degradation and catalysis is complex PC^{+}/Br^{-} , produced by the reductive initiation of the DPP catalyst and the initiator (Scheme 1). This complex undergoes degradation through reactive oxygen species while simultaneously being oxidatively quenched by propagated polymer chain radicals. Consequently, pure polymer production with ultra-high

molecular weight (UHMW) has been realized through simultaneous regulation of both the lifetime of polymer chain radicals and the degradation rate of complex PC^{+}/Br^{-} during photopolymerization. This approach is not only feasible but also scientifically justifiable.

Results and Discussion



Scheme 1 Comparison of previously reported photo-ATRP system and our work. Schematic processes and principals for combining photopolymerization and self-degradation with DPP as the organo-photocatalyst (PC).

In recent years, photopolymerization has emerged as a valuable supplement to conventional polymerization due to its capability to offer control over light, time, and spatial aspects alongside its mild operation conditions. Organic photocatalysts offer several advantages, such as environmental friendliness and precise control over product composition and distribution. However, the utilization of organic catalysts can potentially introduce color, unknown toxicity, and exhibit relatively low initiation efficiency. To address these issues, we propose a concept where the organo-catalysts undergo self-degradation subsequent to initiation, thereby enhancing the potential applications of the resulting polymers. The entire process and idea were illustrated in Scheme 1 (bottom). Specifically, DPP catalysts can be excited by photo energy, generating highly reductive lowest unoccupied molecular orbital (LUMO) and electron-deficient highest occupied molecular orbital (HOMO). Initiation in photopolymerization relies on the reductive dehalogenation of an alkyl halide initiator via outer-sphere electron transfer from a photoexcited organic catalyst.¹⁸ In the reductive initiation pathway, when the PCs become photoexcited by light irradiation, they generated the strongly reducing excited state (PC^*), which will directly reduce the initiator, producing reactive carbon radicals to initiate the monomers, thereby initiating polymer chain propagation. After reacting with the initiator, the electron-deficient PC cation radical (PC^+) composited with the bromine anion (Br^-) simultaneously to form the intermediate PC^+/Br^- complex.¹¹⁻¹² This complex plays a crucial role in polymer chain growth by tending to deactivate the propagating polymer chain radicals and cause

termination of propagation. Simultaneously, this complex undergoes another pathway where it can be degraded by highly reactive oxygen species, resulting in mineralization into small molecules. Consequently, the degradation of unstable PC complex intermediate dramatically affects the termination of the propagating polymer chain and consequently influences the final polymer product.

Regarding the reactive oxygen species acting degradation, the excited DPP undergoes electron/energy transfer reactions with O_2 and H_2O , generating singlet oxygen (1O_2), superoxide radical ($O_2^{\cdot-}$), and hydroxyl radical ($\cdot OH$) species. These resultant species exhibit highly oxidizing activity on the unstable PC^+/Br^- complex, thereby contributing to the self-degradation of DPP.¹⁹ This process allows for effective control over the initiation and degradation of organo-photocatalysts through the application of photopolymerization techniques, thus facilitating the production of pure polymers.

In this study, we extensively investigated the photophysical and electrochemical properties of DPP compounds, as well as exploring both the steady-state and reactive species in DPP solutions. Furthermore, we have revealed the kinetics and thermodynamics governing DPP degradation and photopolymerization.

Photocatalyst Characteristics

Photophysical characteristics. The careful selection of appropriate compounds is pivotal in achieving a delicate equilibrium between DPP degradation and DPP catalysis, as both processes are substantially influenced by the stability of molecular structure and the efficient electrons/energy transfer to initiators. Two DPP catalysts were meticulously chosen to conduct photopolymerization in comparison: phenyl DPP (**PhDPP**) and thiophene DPP (**TDPP**).¹⁶ The optical properties of N-H unsubstituted DPPs were characterized using UV-vis and steady-state fluorescence spectroscopy, as shown in Fig. 1a and collected in Table 1. As expected, both DPPs showed strong absorption in the visible-light region. **TDPP** functionalized with thiophene-functionalized²⁰⁻²¹, exhibited maximum absorbance at 528 nm, featuring two shoulder peaks at 491 nm and 460 nm. While **PhDPP** displayed an absorbance peak at 503 nm, with two shoulder peaks at 469 nm and 441 nm, respectively. The presence of shoulder peaks typically indicates H-aggregation caused by π - π stacking, which strengthens the excited-state DPP molecular interaction and facilitates the degradation itself.²² Notably, the fluorescence spectra of each DPP derivative exhibited mirrored its absorption spectrum, indicating vibronic transitions arising from similar energy level distributions in the ground state and the first excited state.²³

The excited states of **TDPP** were further investigated using femtosecond time-resolved transient absorption (fs-TA) spectroscopy in DMF solution (10^{-4} M), which revealed distinct ground-state bleaching (GSB), stimulated emission, and photo-induced absorbance (Fig. 1b). Specifically, the photo-induced absorbance was assigned to singlet excited state absorption at 750 nm, exhibiting a sharp positive peak that initially increased in intensity for several picoseconds (ps) before decaying as the GSB decreased. The spectrum also showed three negative peaks at around 490 nm, 530 nm, and

580 nm, corresponding to the GSB effect,²⁴⁻²⁵ while the feature at 580 nm ascribed to stimulated emission. Notably, even at 3 ns, the spectrum retained three negative peaks at 490 nm, 530 nm, and 580 nm, alongside positive peaks around 750 nm, strongly indicating the presence of a triplet state of **TDPP**.²⁶⁻²⁷ Moreover, the time-resolved fluorescence of DPP in DMF solution was measured to determine the excited-state lifetime (Fig. 1c), yielding values of 5.75 ns for **TDPP** and 5.92 ns for **PhDPP**, respectively, as summarized in Table 1. The absolute quantum yields provided further evidence of the extended lifetimes of excited-state **DPP**, rendering them suitable for photogenerated catalysis. These findings lay the groundwork for reduction reactions involving substrates through efficient energy and electron transfer processes.

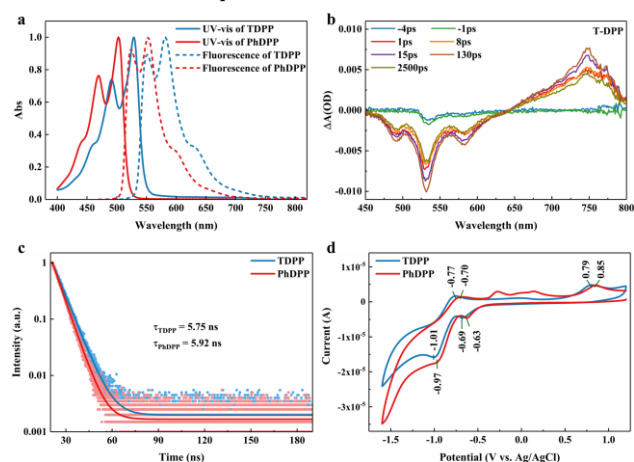


Fig. 1 Photophysical and electrochemical properties of catalysts **TDPP** and **PhDPP**. Normalized absorption and fluorescence spectra (a, DMF, 2.5×10^{-5} mol·L⁻¹, excitation at 450 nm), transient absorption (b), transient fluorescence (c), and electrochemical cyclic voltammograms (d) at the scanning rate of 100 mV s⁻¹.

Electrochemical characteristics. The electrochemical redox characteristics of **TDPP** and **PhDPP** were evaluated using cyclic voltammetry (CV) tests conducted at the scan rate of 100 mV s⁻¹.²⁸ Illustrated in Fig. 1d, **TDPP** and **PhDPP** exhibited similar redox characteristics, featuring two sets of reversible oxidation and reduction peaks. For **TDPP**, the reduction peaks were situated at -0.69 V and -1.01 V, while for **PhDPP**, those peaks were located at -0.63 V and -0.97 V. On the other hand, the oxidation peaks were located at -0.77 V and 0.79 V for **TDPP** and -0.70 V and 0.85 V for **PhDPP**, respectively. Additionally, the reducing potential of these catalysts in their excited state ($E^{0*}(PC^+/PC^*)$) was assessed based on fluorescence emission and the onset potential of oxidation (as detailed in Table S1). **TDPP** exhibited a reducing potential ($E^{0*}(PC^+/PC^*)$) of -1.42 V, while **PhDPP** had a reducing potential of -1.52 V. Despite the excited states of both **TDPP** and **PhDPP** being less reductive compared to commonly used metal PCs, such as fac-Ir(ppy)₃ (-1.73 V vs SCE),²⁹⁻³⁰ these DPP derivatives still demonstrated the capability to reduce ethyl 2-bromoisobutyrate (EBiB, a commonly used initiator). These findings provide significant insight into the reducing capabilities of the DPP catalysts in their excited states.

Table 1 Photophysical, redox, and excited-state properties of **TDPP** and **PhDPP**.

PC	λ_{abs} (nm)	λ_{em} (nm)	ϵ ($\text{L} \cdot (\text{mol} \cdot \text{cm})^{-1}$)	τ^a (ns)	QY ^b	E ^c (V)
TDPP	528	581	3.64×10^4	5.748	83.6%	-1.42
PhDPP	503	553	3.6×10^4	5.923	98.0%	-1.52

λ_{abs} , Absorption maximum; λ_{em} , Emission maximum; ϵ , Extinction coefficient. ^aThe excited state singlet lifetime of DPP in DMF (10^{-5} M). Excitation: 450 nm. ^bThe absolute quantum yield without using reference. ^c Calculated the excited state reduction potentials.

Photopolymerization Reactions and Polymer Properties

Polymer Properties. Before systematically exploring the photocatalytic performance of DPP in a photopolymerization system, we conducted preliminary control experiments to validate the catalytic role of DPP in polymerization (entries 18~23 in Table 2 and entries 4, 5, 9, 10 in Table S2). Methyl methacrylate (MMA) and styrene (St) were selected as the model monomers. The number-average molecular weights (M_n) increased over extended reaction times. Both **TDPP** and **PhDPP** demonstrated effective catalytic activity in photopolymerization, producing high molecular weight (M_n) PMMA with substantial monomer conversion and low dispersity (M_w/M_n) ranging from 1.3 to 2.6. The photopolymerization process could also be effectively conducted with different initiators (Fig. S2) or under white light irradiation (Table S2). Incorporating cross-linking agents (ethylene glycol dimethacrylate, EGDMA) into the reaction system significantly enhanced MMA conversions as high as 98%, which exhibited promising potential application in photo printing. Particularly noteworthy was the achievement of monomer conversion > 95% for MMA with **TDPP** catalyst, leading to the production of ultra-high molecular weight PMMA (709.9 kDa, entry 6). Notably, employing the **PhDPP** catalyst resulted in PMMA with an M_n as high as 2106.5 kDa (entry 12 and Fig. S3), marking the highest M_n of PMMA ever reported in photopolymerization (Table 3).³¹⁻³² The PMMA with UHMW led to the reaction solution transitioning into a translucent gel (Fig. S1, S2) with certain elasticity (Fig. S3). Furthermore, the gel could also be obtained without the addition of a solvent, suggesting the potential application of this photopolymerization technique in 3D photocuring, especially upon copolymerized with cross-linkable monomers. The attainment of high-purity terminal polymers from the photocuring reaction is crucial for the successful implementation of 3D photopolymerization.³³ Notably, in this research, the produced polymer gels and PMMA/PS powders were obtained without any catalyst residues, confirmed by ¹H-NMR

(refer to Fig. 2, Fig. S7-S14).³⁴⁻³⁵ As seen in Fig. 2, PMMA and PS samples precipitated from methanol directly without any purification, exhibiting typical features of PMMA and PS without any impurity. These results collectively confirmed the effective catalytic role of **TDPP** and **PhDPP** in photopolymerization for high-purity polymers with ultra-high molecular weights.

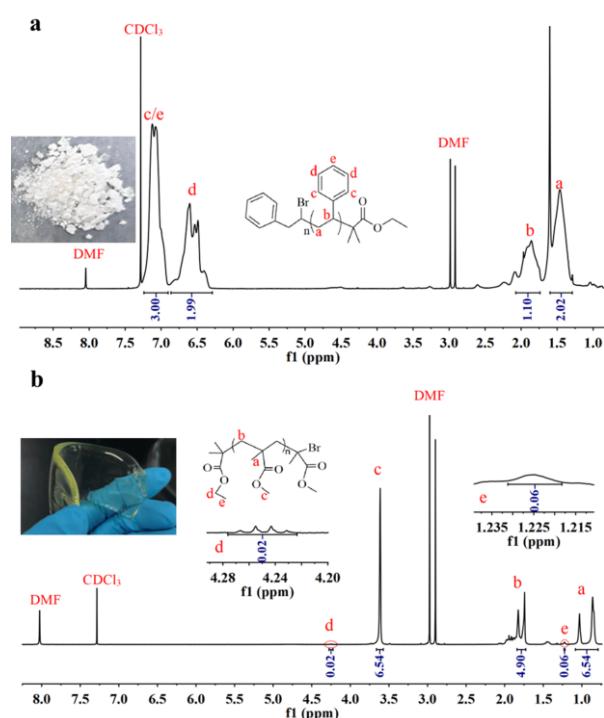


Fig. 2 ¹H-NMR spectra of PMMA and PS prepared by DPP catalyzed photopolymerization without purification. (a) **TDPP** catalytic reaction for 4 hours; (b) **PhDPP** catalytic reaction for 6h).

Table 2 Results of the polymerization of methyl methacrylate (MMA) and styrene (St) using **TDPP** and **PhDPP** as the photocatalysts.

entry	PC	Monomer	Initiator	Time (h)	Conv. ^b (%)	M_n^c (kDa)	M_w/M_n^c
1	TDPP	MMA	EBiB	2	8.51	90.3	1.65
2	TDPP	MMA	EBiB	3	16.78	101.2	1.58
3	TDPP	MMA	EBiB	4	26.45	112.5	1.73
4	TDPP	MMA	EBiB	5	32.19	121.8	1.65
5	TDPP	MMA	EBiB	6	36.13	133.3	1.52
6	TDPP	MMA	EBiB ^a	6+12	95.23	709.9	1.87
7	PhDPP	MMA	EBiB	2	8.84	100.9	1.58
8	PhDPP	MMA	EBiB	3	17.11	119.5	1.79

9	PhDPP	MMA	EBiB	4	26.7	122.6	2.55
10	PhDPP	MMA	EBiB	5	32.19	128.7	2.56
11	PhDPP	MMA	EBiB	6	34.51	135.1	1.54
12	PhDPP	MMA	EBiB ^a	6+12	50.68	2106.5	1.38
13	TDPP	St	EBiB	4	4.60	16.3	1.84
14	TDPP	St	EBiB	6	10.10	21.9	2.12
15	PhDPP	St	EBiB	3	1.16	18.9	2.03
16	PhDPP	St	EBiB	4	2.67	23.4	1.95
17	PhDPP	St	EBiB	6	12.37	41.4	1.95
18	TDPP	MMA	-	6	-	-	-
19	PhDPP	MMA	-	6	-	-	-
20	TDPP	St	-	6	-	-	-
21	PhDPP	St	-	6	-	-	-
22	-	MMA	EBiB	6	-	-	-
23	-	St	EBiB	6	-	-	-

Note: DMF (10 mL) served as the solvent in a quartz bottle (50 mL), and the reaction ingredients were: [C] / [I] / [M] = 0.01: 7: 100 at room temperature under blue light (450 nm, 20W).

^a [C] / [I] / [M] = 0.01: 0.7: 100. 6h light irradiation followed by 12h dark reaction. [C], [I], and [M] represent the concentrations of catalyst, initiator, and monomer, respectively. ^b Determined gravimetrically. ^c Molecular weight and polydispersity were determined by gel permeation chromatography (GPC), using THF as eluent.

Table 3 Comparative results of the O-ATRP mediated by different metal-free photocatalysts (PCs).

PC	Monomer (M)	M _n (kDa)	M _w /M _n	Time (h)	Light	[C]/[I]/[M] ^a	Refs
DPP	MMA	2106.5	1.38	6+12 (dark)	450 nm	0.01:0.7:100	This work
TTBP	MMA	46.0	1.80	4	450 nm	1:75:550	¹⁴
diphenyl dihydrophenazine	MMA	17.9	1.17	8	sunlight	1:10:1000	³⁶
O-doped anthanthrene	MMA	14.9	1.23	10	400 nm	0.5:1:100	³⁷
Eosin Y	MMA	15.1	1.33	2	400~500 nm	0.1:1:200	³⁸
Erythrosin B	MMA	90.0	1.20	2	400~500 nm	0.1:1:200	³⁸
TBOC-QA	MMA	43.7	1.55	10	Blue light	0.4:1:200	³⁹
Pyrene	MMA	16.4	1.5	2	350 nm	1:0.1:100	⁴⁰
perylene	MMA	11.9	1.82	6	400-700 nm	1:10:1000	⁴¹ ⁴²
TT-TPA	MMA	31.2	1.35	4	350 nm	0.125:0.25:100	⁴³
phenoxazine	DBMM/MMA	8.0	1.22	24	White light	1:10:1000	⁴⁴
phenylphenothiazine	MMA	15.4	1.32	7	380 nm	1:1:1000	⁴⁵

^a [C], [I], and [M] represent the concentrations of catalyst, initiator, and monomer, respectively.

Polymerization kinetics. To confirm the temporal control role of light in polymerization propagation, a pulsed light sequence was conducted. A cyclic pattern of 1 h of irradiation followed by an hour of the dark period was performed using a reactant ratio of [PC]: [EBiB]: [MMA] = 0.01:0.7:100. This experimental procedure conclusively established that polymerization propagation strictly proceeded during light irradiation,

with no discernible monomer consumption observed during the dark periods (Fig. 3 and S7). Notably, the high chain-end fidelity was also confirmed by the polymer structural analysis of ¹H-NMR (Fig. S8-S15). Meanwhile, the polymerization gradually decelerated after 6 hours due to the self-degradation of photocatalysts and the real-time consumption of monomers throughout the polymerization process. Moreover, this

polymerizing technique and light-controlled effect also applied to other monomers and block copolymer, e.g., acrylate, acrylic, styrene, and acrylonitrile, showing broad monomer applicability (Fig. 3c and 3d).

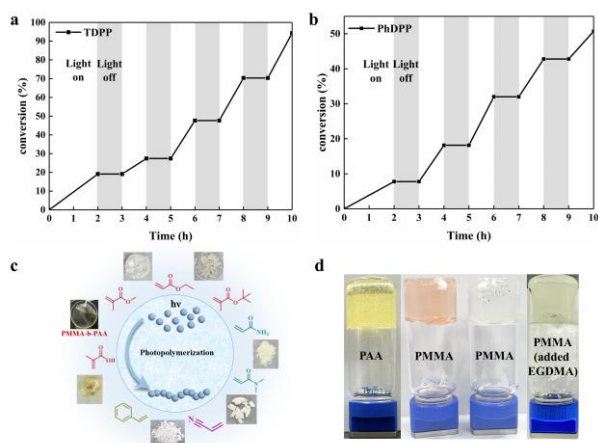


Fig. 3 Temporal control of photopolymerization and monomer conversion versus time in the synthesis of PMMA (a, b) using **TDPP** and **PhDPP** as catalysts under blue-light LED irradiation. (c) Different monomers are applicable in this photoinitiation system. (Catalyst: 0.15 mg/mL; monomer: initiator = 100: 0.7; 450nm). (d) Photographs of gelatinous reaction systems catalysed by DPPs.

The kinetics of the photopolymerization process were further analyzed and presented in Fig. 4. The GPC elution traces (Fig. 4a, S5a, and S6) notably displayed a shift to the higher molecular species, suggesting the chain extension during

polymerization.⁷ Detailed kinetic plots of $\ln([M]_0/[M]_t)$ over time (Fig. 4b) revealed the first-order kinetic of the reaction process, signifying that the rate of monomer consumption was proportional to the remaining monomer concentration throughout the polymerization. Fig. 4c and Fig. S5b illustrate a linear increase in the number-average molecular weight (M_n) of the resulting polymer as the monomer conversion proceeded for both **TDPP** and **PhDPP**. Notably, the molecular dispersion (M_w/M_n) showed a tendency to decrease after the monomer conversion reached around 30%, likely attributed to the bimolecular termination of short polymer propagating chains. This aspect also contributes to the achievement of the ultra-high molecular weight (UHMW) characteristic. Moreover, as observed in Figures 4d and 4f, the polymer chains underwent continuous growth even after cessation of the light irradiation. 6h light irradiation on the starting reaction system yielded the complete degradation of DPPs and simultaneously a transparent polymer solution with M_n value of 189.2 kDa. Subsequent 12h dark reaction led continuous polymerization of MMA and produced PMMA with higher molecular weight of 2,106.5 kDa. This significant discovery highlighted the persistent activity of polymer radicals and their crucial role in achieving PMMA with ultra-high molecular weight (UHMW). Consequently, the polymerization reaction continued after DPPs were completely degraded, facilitating uninterrupted growth of the polymer chains. Overall, the analysis of photopolymerization kinetics provided valuable insights into polymer chain growth and molecular weight distribution, confirming the effectiveness of **TDPP** and **PhDPP** catalysis in facilitating light-initiated controlled polymerization with ultra-high molecular weight.

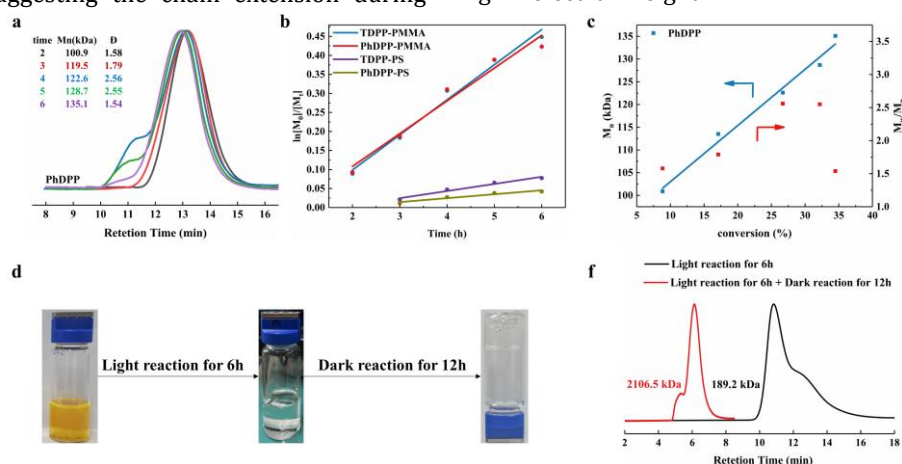


Fig. 4 Molecular weight distribution (MWDs) of PMMA prepared using **PhDPP** (a). The kinetic plot of $\ln([M]_0/[M]_t)$ versus exposure time using various DPP concentrations under N_2 (b). The plot of M_n and \bar{D} (M_w/M_n) vs monomer conversion for the polymerization of MMA under continuous irradiation (c). (Catalyst: 0.15 mg/mL; monomer: initiator = 100: 7; blue light). The experimental process of light/dark reaction (d) and the responding molecular weight distributions (MWDs) (f). (Catalyst: 0.15 mg/mL; monomer: initiator = 100: 0.7; blue light).

Reaction Mechanism

Kinetics of photocatalytic DPP self-degradation. The assessment of DPP degradation was conducted by monitoring the gradual reduction in the absorption maximum at 528 nm for **TDPP** and 503 nm for **PhDPP**, respectively, observed through UV-vis spectroscopy.⁴⁶ To capture the active species generated during the degradation process, various quenchers were introduced, as shown in Fig. 5. Specifically, phenol, TEMPO, carotene, and high-concentration sorbitol acted as h^+ ,

$\bullet OH$, 1O_2 , and triplet-state scavengers were utilized, respectively.⁴⁷⁻⁴⁸

The degradation process of DPP derivatives (10~50 ppm) could be completely accomplished within a 40-minute duration. However, the addition of quenchers slowed down the rates of photocatalytic degradation, resulting in degradation rates ranging from 0.011 to 0.092 for **TDPP** and from 0.009 to 0.120 for **PhDPP**, respectively. The introduction of quenchers effectively regulated the degradation rates, highlighting the role of specific reactive species, including h^+ , $\bullet OH$, 1O_2 , $O_2^{\bullet -}$, and

triplet states in the degradation process.⁴⁹ In particular, when N₂ and TEMPO were present simultaneously, the degradation rate constants decreased to 0.012 for **TDPP** and 0.009 for **PhDPP**, respectively. This pointed towards the participation of oxygen (O₂) gas as a crucial factor in the degradation, which also played a significant role in controlling the photopolymerization reaction as a radical quencher. Noticeably, the additive EBiB, functioning as an initiator for photopolymerization, should react with the singlet-state DPP through one-electron transfer to form carbon radical (C[•]) and DPP complex (DPP^{•+}/Br⁻), yet it did not exhibit any effect on the degradation kinetics. This strongly suggests that intermediate complex DPP^{•+}/Br⁻ could also undergo degradation like the DPP precursor.

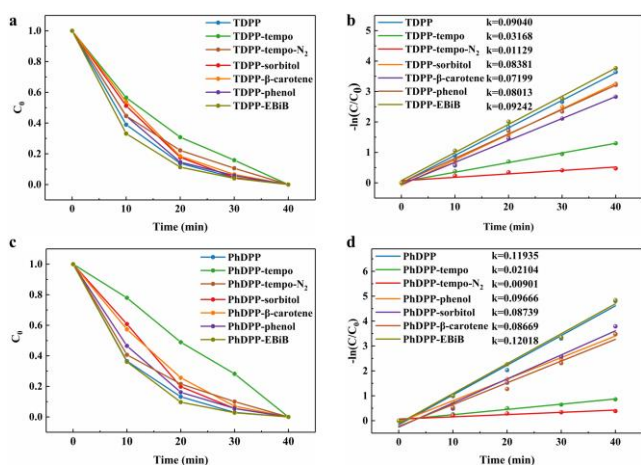


Fig. 5 Photo-initiated degradation of **TDPP** and **PhDPP** (10 ppm in DMF, blue light) under different additives and the corresponding degradation rate constants.

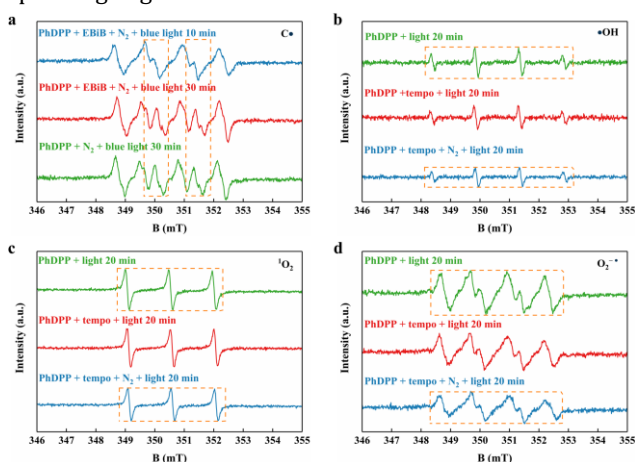


Fig. 6 EPR-trapping tests for different radicals and ROS under DPP degradation systems with DMPO as the scavenger (TEMPO for ¹O₂).

Furthermore, electron spin resonance (EPR) trapping was conducted to directly validate the generation of reactive oxygen species (ROS) and radicals in photocatalysis.⁴⁹⁻⁵⁰ In the case of **PhDPP** solution, EPR signals corresponding to carbon radicals (C[•]), •OH radicals, singlet oxygen (¹O₂), and superoxide radicals (O₂^{•-}) were all detected during light irradiation (Fig. 6, S16 and S17). Upon light irradiation of 30 minutes, carbon radical (C[•]) was detected, indicating the production of C[•] during the decomposition process of DPP (Fig. 6a). Similar

signals were also found after the addition of initiator EBiB. Especially, the peak signals changed significantly between 10 min- and 30 min-irradiation, demonstrating the involvement of EBiB in C[•] generation, which serves as the radical to make the photopolymerization of monomers proceed and undergoes degradation itself during light irradiation. Another possibility of this time-dependent EPR signal change is the involvement of Br⁻ in formation of DPP^{•+}/Br⁻, which would be cross corroborated in the following parts.⁵¹⁻⁵² The typical 1:2:2:1 signal in Fig. 6b demonstrated photocatalytic production of •OH radical by DPP.⁵³ Clearly, adding TEMPO showed no impact on the generation of •OH radicals, as they result from the reaction of holes (h⁺) with water molecules (H₂O). Additionally, Fig. 6c depicted the typical 1:1:1 singlet oxygen (¹O₂) deriving from the excited triplet states of DPP.⁵⁴ The superoxide radical (O₂^{•-}) signal was also detected in Fig. 6d, and the TEMPO addition exhibited little impact on the O₂^{•-} output. It is noteworthy that after the nitrogen-gas purging, all ROS signals observed were notably reduced, once again highlighting the significant role of oxygen in the degradation process.⁵⁵ These results directly confirmed the generation of ROS and radicals during the DPP photocatalysis, supporting their involvement in the self-degradation of DPP and the initiation of the photopolymerization process.

Thermodynamics and mechanism of photocatalytic DPP self-degradation.

The investigation into the thermodynamics of photocatalytic self-degradation of DPP was conducted to examine the catalysis mechanism.⁵⁶ Specifically, the degradation of TDPP and PhDPP, both in the absence and presence of initiator EBiB, were conducted across different solution temperatures. The first-order rate constant (k) was determined by the change of the absorption maximum (Fig. 7a and Fig. S18) upon light-irradiated degradation. Subsequently, utilizing the linear representation of the Arrhenius equation (equation 1), ln k was plotted against 1/T (Fig. 7b and 7c). The intercept and slope were used to derive the values of activation energy (E_{act}), as shown in Table S3. More information can be found in the *Supporting Information*.

$$\ln k = -\left(\frac{1}{T}\right) \times \left(\frac{E_{\text{act}}}{R}\right) + \ln A \quad (1)$$

The k values ranged from 0.101 min⁻¹ to 0.122 min⁻¹ for **TDPP** and from 0.133 min⁻¹ to 0.169 min⁻¹ for **PhDPP**, respectively. These observed variations in values of the rate constant k underscore the impact of temperature on the degradation process. The enhanced photocatalytic degradation activity at elevated temperatures was most likely ascribed to the thermal-induced acceleration of molecular movements. Of particular attention, following the addition of EBiB, the k values ranged from 0.134 min⁻¹ to 0.193 min⁻¹ for **TDPP** and from 0.163 min⁻¹ to 0.210 min⁻¹ for **PhDPP**, respectively. The activation energy (E_{act}) changed from 5.04 kJ mol⁻¹ to 9.50 kJ mol⁻¹ for **TDPP** and from 6.19 kJ mol⁻¹ to 6.54 kJ mol⁻¹ for **PhDPP**, respectively. The rise in the activation energies (Fig. 7d) is attributed to the change of involved degraded species from DPP to DPP complex (DPP^{•+}/Br⁻) subsequent to the addition of initiator EBiB, as employed in the photopolymerization. It is critical to note that the degradation reaction was non-spontaneous, as evidenced by the positive values of the free energy change (ΔG) listed in Table S3. Consequently, these reactions required external photo energy input to initiate the

degradation, and the direct involvement of the DPP complex ($\text{DPP}^{2+}/\text{Br}^-$) was imperative.

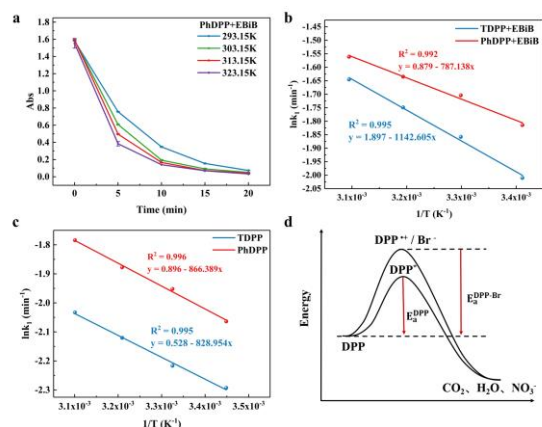
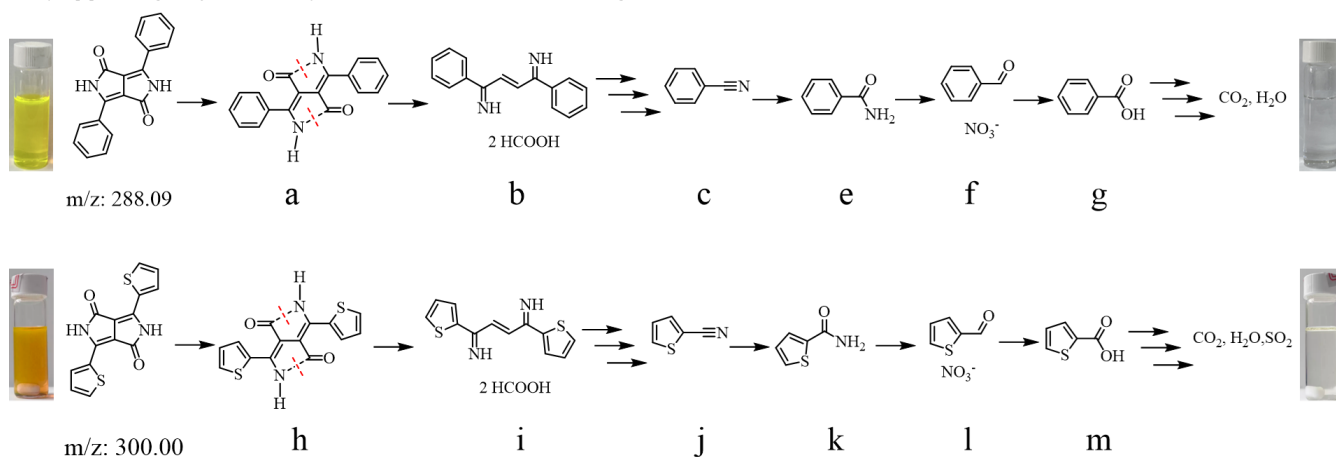


Fig. 7 Degradation of **PhDPP** and **EBiB** (a) at different temperatures under 450 nm and the temperature dependency of degradation rate (b), the plot of $\ln k$ (min^{-1}) against $1/T$ (K^{-1}). Degradation rates (c) of **TDPP** and **PhDPP** at different temperatures under 450 nm, the plot of $\ln k$ (min^{-1}) against $1/T$ (K^{-1}). (d) The comparison of activation energy in photodegradation between DPP^* and $\text{DPP}^{2+}/\text{Br}^-$.

For a more comprehensive understanding of the degradation species, the DPP solutions were subjected to GC-MS analysis (*Supporting Information*) both before and after light

exposure. As depicted in Scheme 2, several small molecules (c-g and j-m) were observed during **TDPP** and **PhDPP** degradation in DMF solvent. Additionally, in an aqueous environment (H_2O), **TDPP** and **PhDPP** were not dissolved and exhibited nanosheet morphology (Fig. S19). Consequently, a gradual reduction in total organic carbon (TOC) was observed during the light irradiation of 5 and 10 hours (as depicted in Fig. S20), confirming gas production and mineralization effects in DPP degradation. To ascertain the primary dissociation site within the DPP molecule, DFT calculations were employed to present electrostatic potential (ESP), frontier orbitals, Fukui function, and Laplacian bond order (Fig. 8). Upon excitation, the electron transition occurred from HOMO to LUMO, locating the least stable part of a molecule. In DPP molecules, HOMO and LUMO were predominantly located on the diketopyrrolopyrrole ring rather than the adjacent group. Moreover, the ESP mapping indicated a distinctive node of positive and negative charge in the diketopyrrolopyrrole ring, specifically between the nitrogen atom and carbon atom ($-\text{C}=\text{O}$).⁵⁷ These features strongly indicated the instability and dissociation tendency of the diketopyrrolopyrrole ring. Furthermore, the smallest Laplacian bond order (0.83) and discrepancy (Δf) of the Fukui function collectively confirmed the specific dissociation site, the N-C ($-\text{C}=\text{O}$) bond, as shown in Scheme 2a and 2h.⁵⁸⁻⁶⁰ The dissociated products (b and i) were further validated through FT-IR spectra (Fig. S21).



Scheme 2 Schematic process of the DPP catalysts self-decomposition.

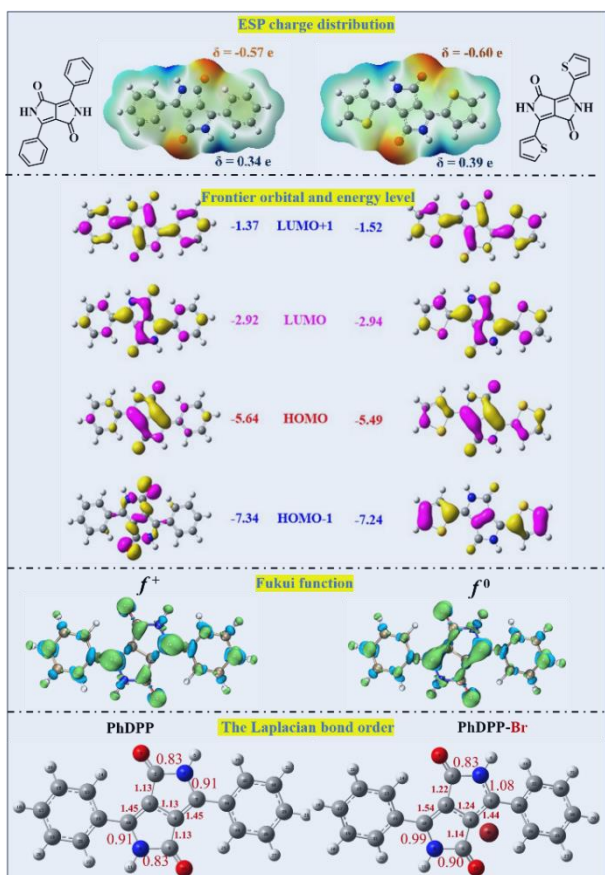


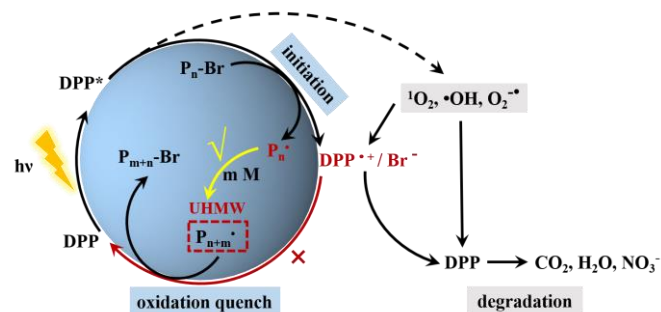
Fig. 8 Charge distribution, frontier orbitals, Fukui function, and Laplacian bond order of organo-photocatalysts **PhDPP** and **TDPP**.

Mechanism of producing pure polymers with ultra-high molecular weight

A comprehensive analysis was conducted to understand the relationship between the self-degradation of DPP and photopolymerization, emphasizing the production of pure polymers featuring UHMW, as illustrated in Scheme 3. Specifically, the DPP catalysts exhibit efficient photon absorption capabilities, becoming excited upon exposure to visible light (DPP^*). Upon photoexcitation, these catalysts yield a strongly reducing excited state ($E_{\text{TDP}} = -1.42\text{V}$ vs Ag/AgCl , $E_{\text{PhDPP}} = -1.52\text{V}$ vs Ag/AgCl), characterized by a sufficiently long lifetime ($\tau_{\text{TDPP}} = 5.75\text{ ns}$, $\tau_{\text{PhDPP}} = 5.92\text{ ns}$) and high quantum efficiency ($QY_{\text{TDPP}} = 0.84$, $QY_{\text{PhDPP}} = 0.98$) (Table 1), ensuring efficient activation of the R-Br bond in an initiator. The alkyl bromide initiators were activated by DPP^* through single-electron transfer, leading to the generation of carbon radicals (C^\bullet) and DPP complex ($\text{DPP}^{+\bullet}/\text{Br}^-$). These carbon radicals (C^\bullet) will initiate monomers repeatedly to produce propagating polymer radicals (P_n^\bullet and P_{n+m}^\bullet), which can also result in back electron transfer (oxidative quenching) with $\text{DPP}^{+\bullet}/\text{Br}^-$, thereby reversibly terminating the polymerization and regenerating the ground-state DPP simultaneously.

As clearly illustrated in Scheme 3, the oxidative quenching effect, stemming from P_{n+m}^\bullet and $\text{P}_{n+m}^\bullet\text{-Br}$, is significantly influenced by the destiny of the complex DPP-Br. This complex effectively interrupts the growth of the polymer chain

by reacting with P_{n+m}^\bullet , resulting in the release of ground-state DPP. In our study, the destiny of DPP-Br is mediated primarily by self-degradation rather than by the oxidative deactivation typical of the polymerization process. In other words, the oxidative degradation process of DPP-Br prevents oxidation quenching and enables continuous addition of monomers to the propagated active polymer chain (P_n^\bullet and P_{n+m}^\bullet) without termination. This mechanism facilitates the formation of pure polymers with ultra-high molecular weight, a comprehensive elucidation of which is presented in this research.



Scheme 3 Illustrated mechanism of producing the pure polymer with ultra-high molecular weight (UHMW) through DPP degradation and photo-initiated polymerization. DPP^* , photoexcited DPP; $\text{P}_n\text{-Br}$ and $\text{P}_{n+m}\text{-Br}$: quenched propagating polymer chain; P_n^\bullet and P_{n+m}^\bullet : active propagating polymer chain; M: monomer; DPP-Br, DPP intermediate after initiation.

Conclusions

The exploration of N-unsubstituted DPP derivatives as highly efficient self-degradable photo-redox catalysts has proven instrumental in mitigating the quenching effect in photopolymerization through self-degradation, enabling the production of pure polymers with ultra-high molecular weight (M_w). By employing significantly low catalyst loadings (50 ~ 150 ppm), the DPP catalysts have demonstrated excellent control over self-degradation and photo-initiation throughout the photopolymerization process across various monomers, consistently yielding translucent PMMA gel features with ultra-high M_w ($M_n > 2000\text{ kDa}$) and low dispersibility ($\mathcal{D} = 1.38$) after 12 h additional dark reaction. In-depth mechanistic investigations have revealed that the intermediate complex $\text{DPP}^{+\bullet}/\text{Br}^-$ conducted two distinct reaction pathways: self-degradation and quenching propagation of polymer chain radical. Consequently, the degradation of the $\text{DPP}^{+\bullet}/\text{Br}^-$ complex prevents propagated polymer chain quenching and prolongs the lifetime of chain radicals, thus resulting in pure polymers with ultra-high M_w . This development obviates the need for additional purification and signifies the capacity to produce UHMW polymer without the necessity for cross-linkable-monomer addition. Foreseeing the potential impact, we anticipate that such DPP photo-redox catalysts, alongside the concept of degradation-inhibited-quench, will significantly contribute to the advancement of light-curing resins and well-defined materials constructed with light-/time-/spatial-control manners, particularly in their applications in 3D photopolymerization.

Conflicts of interest

There are no conflicts to declare.

Acknowledgements

The authors are grateful to the National Natural Science Foundation of China (No. 22102134), the Natural Science Foundation of Sichuan Province (No. 2022NSFSC0195), the Leader Project at the Korea Institute of Energy Technology (KENTECH) funded by the Ministry of Science and ICT through the National Research Foundation of Korea (No. 2020R1A3B3079715) and the Brain Pool Program by National Research Foundation of Korea (No. 2021H1D3A2A02085101).

Notes and references

- Zhang, J.; Xiao, P., 3D printing of photopolymers. *Polym. Chem-uk* **2018**, *9* (13), 1530-1540.
- Rusling, J. F., Developing microfluidic sensing devices using 3D printing. *ACS Sens.* **2018**, *3* (3), 522-526.
- MacDonald, E.; Wicker, R., Multiprocess 3D printing for increasing component functionality. *Science* **2016**, *353* (6307), 1512-1511.
- Zhu, G.; Houck, H. A.; Spiegel, C. A.; Selhuber-Unkel, C.; Hou, Y.; Blasco, E., Introducing dynamic bonds in light-based 3D printing. *Adv. Funct. Mater.* **2023**, *2300456*, 1-22.
- Bao, Y., Recent trends in advanced photoinitiators for vat photopolymerization 3D printing. *Macromol. Rapid Commun.* **2022**, *43* (14), 202-216.
- Ahn, D.; Stevens, L. M.; Zhou, K.; Page, Z. A., Rapid high-resolution visible light 3D printing. *ACS Cent. Sci.* **2020**, *6* (9), 1555-1563.
- Qiao, L.; Zhou, M.; Shi, G.; Cui, Z.; Zhang, X.; Fu, P.; Liu, M.; Qiao, X.; He, Y.; Pang, X., Ultrafast visible-light-induced ATRP in aqueous media with carbon quantum dots as the catalyst and its application for 3D printing. *J. Am. Chem. Soc.* **2022**, *144* (22), 9817-9826.
- Zhang, Z.; Corrigan, N.; Boyer, C., A photoinduced dual-wavelength approach for 3D printing and self-healing of thermosetting materials. *Angew. Chem. Int. Ed.* **2022**, *61* (11), e202114111 (1 of 9).
- Quirós-Montes, L.; Carriedo, G. A.; García-Álvarez, J.; Presa Soto, A., Deep eutectic solvents for Cu-catalysed ARGET ATRP under an air atmosphere: a sustainable and efficient route to poly(methyl methacrylate) using a recyclable Cu(II) metal-organic framework. *Green Chem.* **2019**, *21* (21), 5865-5875.
- Corrigan, N.; Shanmugam, S.; Xu, J.; Boyer, C., Photocatalysis in organic and polymer synthesis. *Chem. Soc. Rev.* **2016**, *45* (22), 6165-6212.
- Corbin, D. A.; Miyake, G. M., Photoinduced organocatalyzed atom transfer radical polymerization (O-ATRP): precision polymer synthesis using organic photoredox catalysis. *Chem. Rev.* **2022**, *122* (2), 1830-1874.
- Pan, X.; Tasdelen, M. A.; Laun, J.; Junkers, T.; Yagci, Y.; Matyjaszewski, K., Photomediated controlled radical polymerization. *Prog. Polym. Sci.* **2016**, *62*, 73-125.
- C., T. J.; H., L. C.; H., Y.; D., R. M.; B., M. C.; M., M. G., Organocatalyzed atom transfer radical polymerization driven by visible light. *Science* **2022**, *352*, 6289.
- Ravetz, B. D.; Pun, A. B.; Churchill, E. M.; Congreve, D. N.; Rovis, T.; Campos, L. M., Photoredox catalysis using infrared light via triplet fusion upconversion. *Nature* **2019**, *565* (7739), 343-346.
- Yang, L.; Huang, Y.; Peng, Y.; Liu, F.; Zhang, Q.; He, H.; Wang, J.; Jiang, L.; Zhou, Y., Pyridine-diketopyrrolopyrrole-based novel metal-free visible-light organophotoredox catalyst for atom-transfer radical polymerization. *J. Phys. Chem. A* **2020**, *124* (6), 1068-1075.
- Yang, L.; Ngo, H. M.; Luo, Y.; Pawar, A. U.; Sivasankaran, R. P.; Ok, K.; Kang, Y. S., Specific active sites of organo-photocatalysts for photo-atom transfer radical polymerization: a combined experimental and theoretical study of N-unsubstituted diketopyrrolopyrrole. *J. Phys. Chem. C* **2022**, *126* (51), 21576-21584.
- Yang, L.; Peng, Y.; Luo, X.; Dan, Y.; Ye, J.; Zhou, Y.; Zou, Z., Beyond C(3N)4 pi-conjugated metal-free polymeric semiconductors for photocatalytic chemical transformations. *Chem. Soc. Rev.* **2021**, *50* (3), 2147-2172.
- Koyama, D.; Dale, H. J. A.; Orr-Ewing, A. J., Ultrafast observation of a photoredox reaction mechanism: photoinitiation in organocatalyzed atom-transfer radical polymerization. *J. Am. Chem. Soc.* **2018**, *140* (4), 1285-1293.
- Shi, H.; Sun, W.; Wang, Q.; Gu, G.; Si, W.; Huang, W.; Zhang, Q.; Dong, X., A thienyl-substituted diketopyrrolopyrrole derivative with efficient reactive oxygen species generation for photodynamic therapy. *ChemPlusChem* **2016**, *81* (6), 515-520.
- Saes, B. W. H.; Lutz, M.; Wienk, M. M.; Meskers, S. C. J.; Janssen, R. A. J., Tuning the optical characteristics of diketopyrrolopyrrole molecules in the solid state by alkyl side chains. *J. Phys. Chem. C* **2020**, *124* (46), 25229-25238.
- Mauck, C. M.; Hartnett, P. E.; Wu, Y.; Miller, C. E.; Marks, T. J.; Wasielewski, M. R., Singlet fission within diketopyrrolopyrrole nanoparticles in water. *Chem. Mater.* **2017**, *29* (16), 6810-6817.
- Liu, Q.; Sun, H.; Ponnappa, S. P.; Feron, K.; Manzhos, S.; Jones, M. W. M.; Bottle, S. E.; Bell, J.; Noh, Y. Y.; Sonar, P., Naphthalene flanked diketopyrrolopyrrole: A new DPP family member and its comparative optoelectronic properties with thiophene- and furan- flanked DPP counterparts. *Org. Electron.* **2019**, *74*, 290-298.
- Wang, Q.; Lenjani, S. V.; Dolynchuk, O.; Scaccabarozzi, A. D.; Komber, H.; Guo, Y.; Günther, F.; Gemming, S.; Magerle, R.; Caironi, M.; Sommer, M., Electron mobility of diketopyrrolopyrrole copolymers is robust against homocoupling defects. *Chem. Mater.* **2021**, *33* (2), 668-677.
- Hartnett, P. E.; Dyar, S. M.; Margulies, E. A.; Shoer, L. E.; Cook, A. W.; Eaton, S. W.; Marks, T. J.; Wasielewski, M. R., Long-lived charge carrier generation in ordered films of a covalent perylenediimide-diketopyrrolopyrrole-perylenediimide molecule. *Chem. Sci.* **2015**, *6* (1), 402-411.
- Keller, B.; Cai, Z.; Muthike, A. K.; Sahu, P. K.; Kim, H.; Eshun, A.; Zimmerman, P. M.; Zhang, D.; Goodson, T., Investigating the optical properties of thiophene additions to s-indacene donors with diketopyrrolopyrrole, isoindigo, and thienothiophene acceptors. *J. Phys. Chem. C* **2018**, *122* (48), 27713-27733.
- Goswami, S.; Winkel, R. W.; Alarous, E.; Ghiviriga, I.; Mohammed, O. F.; Schanze, K. S., Photophysics of organometallic platinum(II) derivatives of the diketopyrrolopyrrole chromophore. *J. Phys. Chem. A* **2014**, *118* (50), 11735-43.
- Papadopoulos, I.; Álvaro-Martins, M. J.; Molina, D.; McCosker, P. M.; Keller, P. A.; Clark, T.; Sastre-Santos, Á.; Guldi, D. M., Solvent-dependent singlet fission in diketopyrrolopyrrole dimers: a mediating charge transfer versus a trapping symmetry-breaking charge separation. *Adv. Energy Mater.* **2020**, *10* (43), 1496-1505.
- Kim, C.; Liu, J.; Lin, J.; Tamayo, A. B.; Walker, B.; Wu, G.; Nguyen, T., Influence of structural variation on the solid-state properties of diketopyrrolopyrrole-based oligophenyleneethylenes: single-crystal structures, thermal properties, optical bandgaps, energy levels, film morphology, and hole mobility. *Chem. Mater.* **2012**, *24* (10), 1699-1709.
- Treat, N. J.; Fors, B. P.; Kramer, J. W.; Christianson, M.; Chiu, C. Y.; Read de Alaniz, J.; Hawker, C. J., Controlled radical polymerization of acrylates regulated by visible light. *ACS Macro Lett.* **2014**, *3* (6), 580-584.
- Fors, B. P.; Hawker, C. J., Control of a living radical polymerization of methacrylates by light. *Angew. Chem. Int. Ed.* **2012**, *51* (35), 8850-8853.
- Chism, K. A.; Corbin, D. A.; Miyake, G. M., Removal of photoredox catalysts from polymers synthesized by organocatalyzed atom transfer radical polymerization. *J. Polym. Sci.* **2022**, *60* (19), 2747-2755.
- Cole, J. P.; Federico, C. R.; Lim, C. H.; Miyake, G. M., Photoinduced organocatalyzed atom transfer radical polymerization using low ppm catalyst loading. *Macromolecules* **2019**, *52* (2), 747-754.
- Li, W.; Wang, M.; Ma, H.; Chapa-Villarreal, F. A.; Lobo, A. O.; Zhang, Y. S., Stereolithography apparatus and digital light processing-based 3D bioprinting for tissue fabrication. *iScience* **2023**, *26* (2), 106039-106059.
- Zhou, L.; Zhang, Z.; Li, M.; Wang, Q.; Gao, J.; Li, K.; Lei, L., Graphitic carbon nitride (g-C₃N₄) as a sustainable heterogeneous photocatalyst for metal free and oxygen-tolerant photo-atom transfer radical polymerization (photo-ATRP). *Green Chem.* **2021**, *23* (23), 9617-9624.
- Szczepaniak, G.; Jeong, J.; Kapil, K.; Dadashi-Silab, S.; Yerneni, S. S.; Ratajczyk, P.; Lathwal, S.; Schild, D. J.; Das, S. R.; Matyjaszewski, K., Open-air green-light-driven ATRP enabled by dual photoredox/copper

- catalysis. *Chem. Sci.* **2022**, *13* (39), 11540-11550.
36. Shanmugam, S.; Boyer, C., Organic photocatalysts for cleaner polymer synthesis. *Science* **2016**, *352*, 1053–1054.
37. Ma, Q.; Song, J.; Zhang, X.; Jiang, Y.; Ji, L.; Liao, S., Metal-free atom transfer radical polymerization with ppm catalyst loading under sunlight. *Nat. Commun.* **2021**, *12* (1), 429-436.
38. Kutahya, C.; Aykac, F. S.; Yilmaz, G.; Yagci, Y., LED and visible light-induced metal free ATRP using reducible dyes in the presence of amines. *Polym. Chem.* **2016**, *7* (39), 6094-6098.
39. Jia, T.; Huang, S.; Bohra, H.; Wang, M., Examining derivatives of quinacridone, diketopyrrolopyrrole and indigo as the visible-light organic photocatalysts for metal-free atom transfer radical polymerization. *Dyes Pigm.* **2019**, *165*, 223-230.
40. Allushi, A.; Jockusch, S.; Yilmaz, G.; Yagci, Y., Photoinitiated metal-free controlled/living radical polymerization using polynuclear aromatic hydrocarbons. *Macromolecules* **2016**, *49* (20), 7785-7792.
41. Ryan, M. D.; Pearson, R. M.; French, T. A.; Miyake, G. M., Impact of light intensity on control in photoinduced organocatalyzed atom transfer radical polymerization. *Macromolecules* **2017**, *50* (12), 4616-4622.
42. Miyake, G. M.; Theriot, J. C., Perylene as an organic photocatalyst for the radical polymerization of functionalized vinyl monomers through oxidative quenching with alkyl bromides and visible light. *Macromolecules* **2014**, *47* (23), 8255-8261.
43. Kutahya, C.; Allushi, A.; Isci, R.; Kreutzer, J.; Ozturk, T.; Yilmaz, G.; Yagci, Y., Photoinduced metal-free atom transfer radical polymerization using highly conjugated thienothiophene derivatives. *Macromolecules* **2017**, *50* (17), 6903-6910.
44. McCarthy, B.; Miyake, G. M., Organocatalyzed atom transfer radical polymerization catalyzed by core modified N-Aryl phenoxazines performed under air. *ACS Macro Lett.* **2018**, *7* (8), 1016-1021.
45. Treat, N. J.; Sprafke, H.; Kramer, J. W.; Clark, P. G.; Barton, B. E.; Read de Alaniz, J.; Fors, B. P.; Hawker, C. J., Metal-free atom transfer radical polymerization. *J. Am. Chem. Soc.* **2014**, *136* (45), 16096–16101.
46. Singh, S.; Srivastava, V. C.; Mall, I. D., Mechanism of dye degradation during electrochemical treatment. *J. Phys. Chem. C* **2013**, *117* (29), 15229-15240.
47. Zhou, H.; Yan, S.; Lian, L.; Song, W., Triplet-state photochemistry of dissolved organic matter: triplet-state energy distribution and surface electric charge conditions. *Environ. Sci. Technol.* **2019**, *53* (5), 2482-2490.
48. Moor, K. J.; Schmitt, M.; Erickson, P. R.; McNeill, K., Sorbic acid as a triplet probe: triplet energy and reactivity with triplet-state dissolved organic matter via $^1\text{O}_2$ phosphorescence. *Environ. Sci. Technol.* **2019**, *53* (14), 8078-8086.
49. Wang, H.; Jiang, S.; Liu, W.; Zhang, X.; Zhang, Q.; Luo, Y.; Xie, Y., Ketones as molecular co-catalysts for boosting exciton-based photocatalytic molecular oxygen activation. *Angew. Chem.* **2020**, *59* (27), 11093-11100.
50. Nardi, G.; Manet, I.; Monti, S.; Miranda, M. A.; Lhiaubet-Vallet, V., Scope and limitations of the TEMPO/EPR method for singlet oxygen detection: the misleading role of electron transfer. *Free Radic. Biol. Med.* **2014**, *77*, 64-70.
51. Tang, B.; Li, W.-L.; Jiao, Y.; Lu, J.-B.; Xu, J.-F.; Wang, Z.; Li, J.; Zhang, X., A supramolecular radical cation: folding-enhanced electrostatic effect for promoting radical-mediated oxidation. *Chem. Sci.* **2018**, *9* (22), 5015-5020.
52. Jiao, Y.; Li, W. L.; Xu, J. F.; Wang, G.; Li, J.; Wang, Z.; Zhang, X., A Supramolecularly Activated Radical Cation for Accelerated Catalytic Oxidation. *Angew. Chem. Int. Edit.* **2016**, *55* (31), 8933-8937.
53. Tzitrinovich, Z.; Lipovsky, A.; Gedanken, A.; Lubart, R., Visible light-induced OH radicals in Ga_2O_3 : an EPR study. *Phys. Chem. Chem. Phys.* **2013**, *15* (31), 12977-12981.
54. Tanaka, S.; Enoki, T.; Imoto, H.; Ooyama, Y.; Ohshita, J.; Kato, T.; Naka, K., Highly efficient singlet oxygen generation and high oxidation resistance enhanced by arsole-polymer-based photosensitizer: application as a recyclable photooxidation catalyst. *Macromolecules* **2020**, *53* (6), 2006-2013.
55. Lehman, S. E.; Morris, A. S.; Mueller, P. S.; Salem, A. K.; Grassian, V. H.; Larsen, S. C., Silica nanoparticle-generated ROS as a predictor of cellular toxicity: mechanistic insights and safety by design. *Environ. Sci.: Nano*, **2016**, *3* (1), 56-66.
56. Sen, S.; Das, C.; Ghosh, N. N.; Baildya, N.; Bhattacharya, S.; Khan, M. A.; Sillanpaa, M.; Biswas, G., Is degradation of dyes even possible without using photocatalysts? - a detailed comparative study. *RSC Adv.* **2022**, *12* (53), 34335-34345.
57. Demircioğlu, Z.; Kaştaş, Ç. A.; Büyükgüngör, O., Theoretical analysis (NBO, NPA, Mulliken population method) and molecular orbital studies (hardness, chemical potential, electrophilicity and Fukui function analysis) of (E)-2-((4-hydroxy-2-methylphenylimino)methyl)-3-methoxyphenol. *J. Mol. Struct.* **2015**, *1091*, 183-195.
58. Lu, T.; Chen, F., Bond order analysis based on the Laplacian of electron density in fuzzy overlap space. *J. Phys. Chem. A* **2013**, *117* (14), 3100-3108.
59. Tiznado, W.; Chamorro, E.; Contreras, R.; Fuentealba, P., Comparison among four different ways to condense the Fukui function. *J. Phys. Chem. A* **2005**, *109* (14), 3220–3224.
60. Isravel, A. D.; Jeyaraj, J. K.; Thangasamy, S.; John, W. J., DFT, NBO, HOMO-LUMO, NCI, stability, Fukui function and hole – electron analyses of tolcapone. *Comput. Theor. Chem.* **2021**, *1202*, 113296-113306.